

Morphological Studies of Solution-Crystallized Thermoplastic Elastomers with Polyethylene Endblocks and a Random-Copolymer Midblock

Jiaqi Yan,^{1†} Byeongdu Lee,² Steven D. Smith³ and Richard J. Spontak^{1,4,*}

¹Department of Chemical & Biomolecular Engineering, North Carolina State University, Raleigh, NC 27695

²Advanced Photon Source, Argonne National Laboratory, Argonne, IL 60439

³Corporate Research and Development, The Procter & Gamble Company, Cincinnati, Ohio 45224

⁴Department of Materials Science & Engineering, North Carolina State University, Raleigh, NC 27695

(submitted to *Macromol. Rapid Communications*)

ABSTRACT

Styrenic thermoplastic elastomers (TPEs) in the form of triblock copolymers possessing glassy endblocks and a rubbery midblock account for the largest global market of TPEs worldwide, and typically rely on microphase separation of the endblocks and the subsequent formation of rigid microdomains to ensure satisfactory network stabilization. In this study, we investigate the morphological characteristics of a relatively new family of crystallizable TPEs that instead consist of polyethylene endblocks and a random-copolymer midblock composed of styrene and (ethylene-*co*-butylene) moieties. Copolymer solutions prepared at logarithmic concentrations in a slightly endblock-selective solvent are subjected to crystallization under different time and temperature conditions to ascertain if copolymer self-assembly is directed by endblock crystallization or vice-versa. According to transmission electron microscopy, semi-crystalline aggregates develop at the lowest solution concentration examined (0.01 wt%), and the size and population of crystals, which dominate the copolymer morphologies, are observed to increase with increasing aging time. Real-space results are correlated with small- and wide-angle X-ray scattering to elucidate the concurrent roles of endblock crystallization and self-assembly of these unique TPEs in solution.

[†] Current address: Research & Development Department, Kraton Corporation, Houston, TX 77084.

* To whom correspondence should be addressed (e-mail: Rich_Spontak@ncsu.edu).

Morphological Studies of Solution-Crystallized Thermoplastic Elastomers with Polyethylene Endblocks and a Random-Copolymer Midblock

Jiaqi Yan,¹ Byeongdu Lee,² Steven D. Smith,³ and Richard J. Spontak^{1,4}

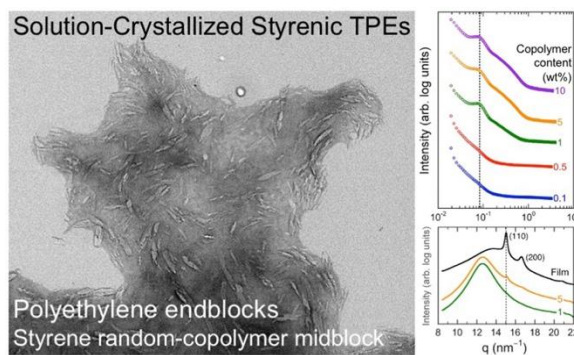
¹Department of Chemical & Biomolecular Engineering, North Carolina State University, Raleigh, NC 27695

²Advanced Photon Source, Argonne National Laboratory, Argonne, IL 60439

³Corporate Research and Development, The Procter & Gamble Company, Cincinnati, Ohio 45224

⁴Department of Materials Science & Engineering, North Carolina State University, Raleigh, NC 27695

For Table of Contents use only



Thermoplastic elastomers (TPEs) combine the melt processability of thermoplastics with the elasticity of elastomers and thus constitute an important category of elastomeric materials, which are becoming increasingly pervasive in a wide range of commodity technologies such as flexible^{1,2} and wearable^{3,4} electronics. Conventional elastomers generated by chemical crosslinking are ubiquitous in a wide range of commercially relevant applications,^{5,6} and advances in quantifying network topologies,⁷ synthesizing materials with tunable properties^{8,9} and adapting these materials to new end uses^{10,11} signify the expanding role of elastomers. The molecular network that develops in these materials is permanent so that (i) shaping must be achieved prior to crosslinking and (ii) post-application disposal often results in solid waste or reprocessed filler. In contrast, TPEs¹² rely on reversible physical crosslinking as a consequence of microphase separation between the incompatible sequences of block polymers.^{13,14} While TPEs are available with different chemical combinations and property sets,^{12,15} styrenic TPEs with a triblock copolymer architecture account for ~1/3 of global TPE production.¹⁶ In this scenario, endblocks typically, but not necessarily,^{17,18} of identical block weight self-assemble into glassy microdomains that serve as physical crosslinks to stabilize a rubbery midblock network.

Most styrenic TPEs consist of endblocks based on atactic polystyrene (S), and the midblocks derive from either a polydiene (polyisoprene or polybutadiene) or its hydrogenated analog, ethylene-*alt*-propylene (EP) or ethylene-*co*-butylene (EB) rubber, respectively. Block-selective hydrogenation greatly increases the interblock thermodynamic incompatibility and significantly elevates the order-disorder transition temperature.^{19,20} One approach to circumvent processing limitations associated with this family of TPEs is to substitute crystallizable hard blocks for the vitrifiable blocks to improve drug delivery,²¹ catalysis,²² optoelectronics,²³ electroactive media,²⁴ and hybrid materials.²⁵ Some crystallizable TPEs possess precise triblock copolymer architectures and

well-defined morphologies due to their synthesis via living anionic polymerization,^{26,27} while others are more accurately described as randomly-coupled multiblock copolymers.^{28,29} Triblock copolymers consisting of linear polyethylene (E) endblocks help to elucidate the competing effects of self-assembly and crystallization on morphology and property development. Myers *et al.*,³⁰ for instance, have reported that TPEs with E endblocks and a hydrogenated poly(5-*n*-hexylnorbornene) midblock exhibit excellent recovery from 200% uniaxial tensile strain. While only bi-component ABA copolymers have been considered thus far, tricomponent ABC copolymers have been synthesized³¹⁻³³ as TPEs with E and S endblocks and a rubbery midblock.

In this study, we focus on examining the solution-crystallized morphologies of two triblock copolymers with E endblocks and a tailorable SEB random-copolymer midblock, which ensures microphase separation due to enhanced interblock incompatibility and the formation of a TPE network with a tunable subambient glass transition temperature (T_g).^{34,35} [To reflect their block architecture, we designate these E-*b*-SEB-*b*-E triblock copolymers as ESEBE.] Our interest in early-stage copolymer crystallization of such copolymers in solution is inspired by the seminal work of Manners and co-workers,^{36,37} who introduced the concept of crystallization-directed self-assembly (CDSA) in crystallizable AB diblock copolymers. According to this mechanism, epitaxial crystallization of crystallizable block polymers promotes the formation of anisotropic assemblies, such as cylindrical micelles instead of traditional nanoscale colloids (*e.g.*, spherical micelles), in the presence of a selective solvent. An intriguing aspect of CDSA is that the anisotropic assemblies can be sonicated to form nucleation seeds from which subsequent crystallization can be controlled in living fashion to yield cylinders with low length dispersity. Combining CDSA with coordination chemistry affords³⁸ a facile and effective means by which to connect such nearly monodisperse building blocks into a variety of multiscale hierarchical structures. To determine if

CDSA governs morphological development in the present copolymers at different solution concentrations and under different aging conditions, we employ transmission electron microscopy (TEM) and synchrotron small- and wide-angle X-ray scattering (SAXS and WAXS, respectively).

A high-temperature proton nuclear magnetic resonance (^1H NMR) spectrum acquired from one of the ESEBE copolymers (ESEBE1) dissolved in *o*-dichlorobenzene is presented in **Figure 1** (see

Table 1 for extracted measurements). The

peaks are labeled according to the chemical

structure of the copolymer. For example, the

two peaks positioned at 7.0-7.3 ppm corre-

spond to the phenyl protons in the S midblock,

while the sharp peak located at 1.4 ppm repre-

sents the CH_2 groups in both the E endblocks

and the EB midblock. The fraction of B units

can be discerned from the peak near 1.0 ppm,

which reflects the presence of methyl end-

groups. Thermal calorimetry, performed on a TA Instruments Q100 unit operated at a heating/

cooling rate of $10\text{ }^\circ\text{C}/\text{min}$, reveals that the melting temperature (T_m) values of the E endblocks are

relatively low ($96.8\text{ }^\circ\text{C}$ for ESEBE1 and $100.0\text{ }^\circ\text{C}$ for ESEBE2, as listed in **Table 1**) due to branch-

ing, which is consistent with a small fraction of B units remaining within the E endblocks after

catalytic hydrogenation of 1,4-butadiene, according to ^1H NMR spectroscopy. In marked contrast,

the EB midblock contains about 40% B. It follows that, in addition to the presence of S in the

midblock, the chemical difference between the E endblocks and the EB midblock is the B content.

Analysis of ^1H NMR spectra in conjunction with results from high-temperature gel

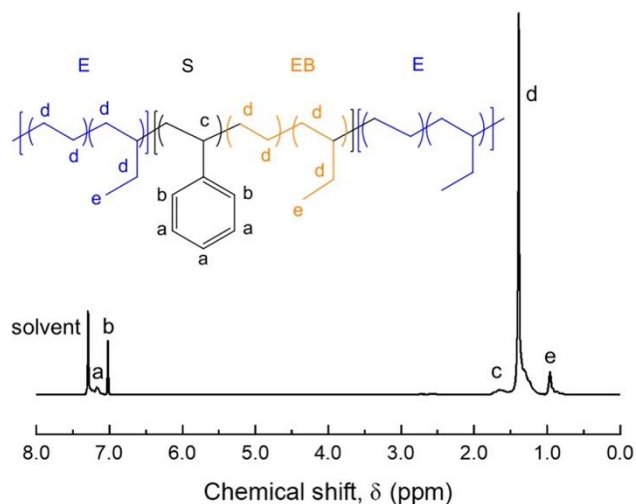


Figure 1. ^1H NMR spectrum acquired from the ESEBE1 copolymer dissolved in *o*-dichlorobenzene at $100\text{ }^\circ\text{C}$. The peaks are labeled according to the chemical structure of the copolymer.

Table 1. Molecular weight and composition characteristics of the ESEBE1 and ESEBE2 triblock copolymers examined in this study.^a

Designation	M _n (kDa)	Đ	Endblocks		Midblock		T _m ^b (°C)	T _c ^b (°C)	T _g ^c (°C)	X _c ^b (%)
			E	B	EB	S				
			(wt%)	(wt%)	(wt%)	(wt%)				
ESEBE1	145	1.45	33.0	4.0	40.5	22.5	96.8	68.7	-35.4	10.1
ESEBE2	109	1.41	30.0	4.0	44.6	21.4	100.0	70.2	-37.2	9.1

^aChemical designations: ethylene (E), butylene (B) and styrene (S).

^bMeasured from melt-crystallized extrudates by DSC.

^cReported by Flood *et al.*³⁹

permeation chromatography (GPC) yields the molecular weight and composition characteristics tabulated for the two block copolymers in **Table 1**. Also included in this table are the T_g³⁹ and crystallization temperature (T_c) values of the copolymers, as well as their degree of crystallinity (X_c) calculated from the measured melting endotherm relative to 100% E (300 J/g). While the two copolymers are chemically identical, they possess modest differences in both number-average molecular weight (M_n) and endblock weight (26.8 kDa in ESEBE1 vs. 18.5 kDa in ESEBE2). Both endblock weights are well above the reported⁴⁰ entanglement molecular weight for E.

Figure 2 displays a pair of TEM images collected from relatively dilute ESEBE1 solutions (0.01 wt% in **Figure 2a** and 0.05 wt% in **Figure 2b**) aged for 1 day at 25 °C in cyclohexane. In these images, the S units are selectively stained and appear electron opaque (dark), whereas E crystals remain unstained. Since the copolymers are dissolved in cyclohexane at 98 °C for 24 h (see the Experimental Section) and since the melting temperatures of the copolymers range from 97 to 100 °C (see **Table 1**), the resulting solutions are expected to be initially structureless. Copolymer self-assembly proceeds upon cooling to ambient temperature since cyclohexane (with a Hildebrand solubility parameter, δ , of 16.8 MPa^{1/2}) is a good solvent for E ($\delta = 16.4$ MPa^{1/2}) but

a poor solvent for S ($\delta = 18.5 \text{ MPa}^{1/2}$).⁴¹ As a consequence, the more solvent-incompatible midblocks are anticipated to self-assemble into cores surrounded by swollen E endblocks, which subsequently crystallize. At the lowest concentration, an irregularly-shaped aggregate surrounded by circular features are evident in **Figure 2a**. Close examination of the aggregate reveals the presence of low-contrast features (presumably thin crystals or E-rich microdomains), some of which indicate radial orientation and others that are parallel to the aggregate surface. The appearance of cusps strongly suggests that crystallization played a nontrivial role in the formation of the aggregate. Cusps, along with much more clearly defined E crystals

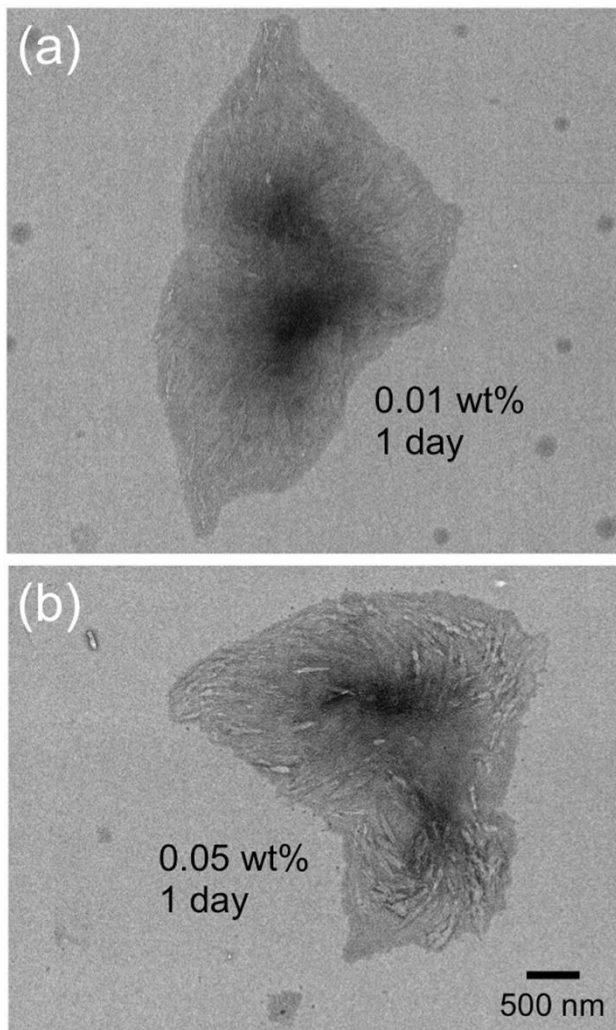


Figure 2. TEM images of the ESEBE1 copolymer prepared at two different solution concentrations (in wt%) – (a) 0.01 and (b) 0.05 – and aged for 1 d at 25 °C.

tals (some of which are oriented within the cusps), are visible in the ESEBE1 copolymer solution-crystallized at a higher concentration in **Figure 2b**. Another feature warranting mention here is the presence of large dark regions, which correspond to out-of-plane features indicative of a complex 3D morphology due to the presence of crystals. Similarly morphologically complex aggregates generated by CDSA have been observed in the case of ABC triblock terpolymers possessing blocks capable of solidifying, one by crystallizing and the other by vitrifying.⁴²

A series of TEM images acquired from the ESEBE1 copolymer prepared from a 0.1 wt% solution aged for different times up to 7 d at 25 °C is provided in **Figure 3**. While discrete aggregates comparable to those seen in **Figure 2** are not observed at this concentration, the specimen immediately quenched to ambient temperature in **Figure 3a** appears discontinuous, resembling a collection of fused aggregates. Scrutinization of this image confirms the existence of crystals, most of which are poorly defined, throughout the specimen. Previous studies have established⁴³ that the morphology of block copolymer aggregates containing crystals is controlled

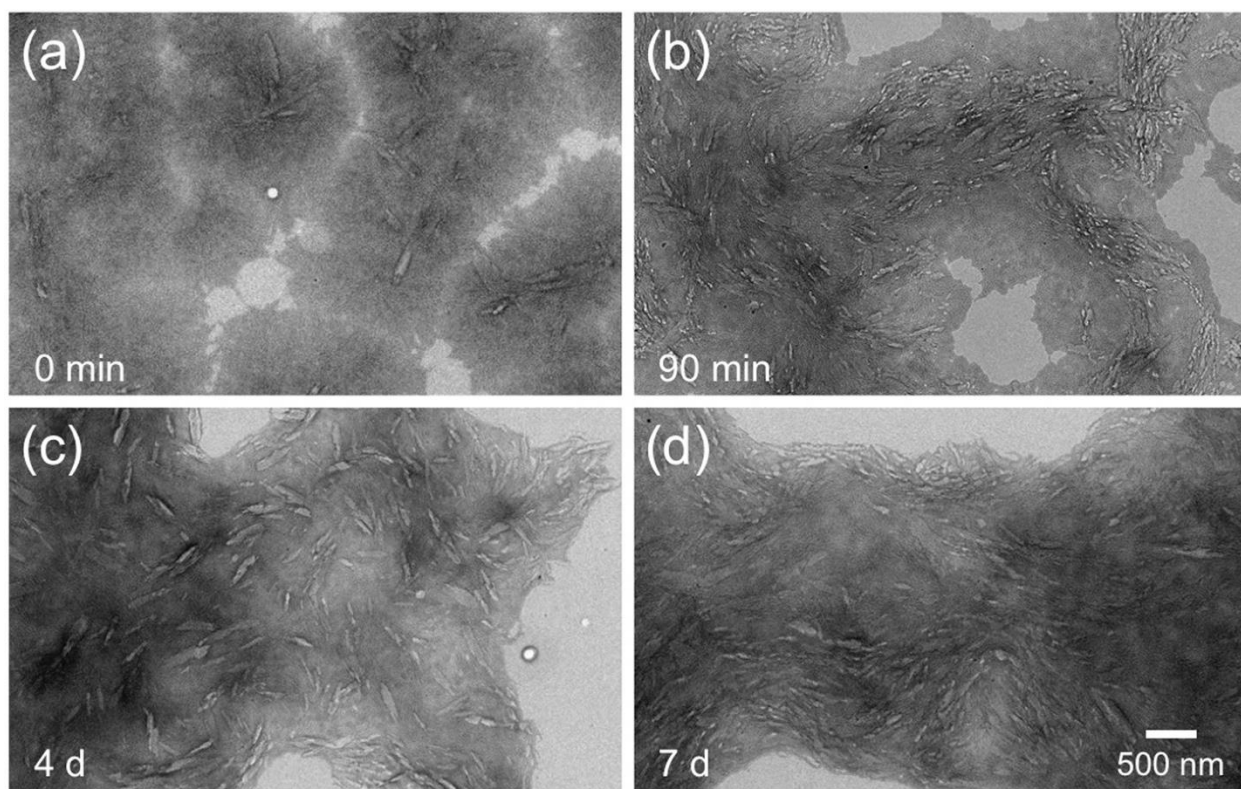


Figure 3. Series of time-resolved TEM images of the ESEBE1 copolymer prepared at a solution concentration of 0.1 wt%, quenched to 25 °C and aged for four different times: (a) 0 min, (b) 90 min, (c) 4 d, and (d) 7 d.

by the interplay of three contributing factors to the free energy: (i) the energy associated with crystal solidification and chain-folding, (ii) the energy due to stretching of the amorphous block, and (iii) the interfacial energy between crystalline and amorphous domains. As in **Figure 2b**, the crystals discernible in **Figure 3a** appear acicular and initially measure *ca.* 160 nm long and 50 nm

wide on average (upon analyzing at least 50 measurements from different images at different magnifications). The population, definition and correlated orientation of the crystals increase substantially after just 90 min in **Figure 3b**. Moreover, the crystal length and width also increase appreciably to *ca.* 240 and 60 nm, respectively. After 4 and 7 d (specimens are pictured in **Figures 3c** and **3d**, respectively), the crystals continue to elongate further to *ca.* 360 (4 d) and 390 (7 d) nm, but the change in thickness is far less pronounced. For completeness,

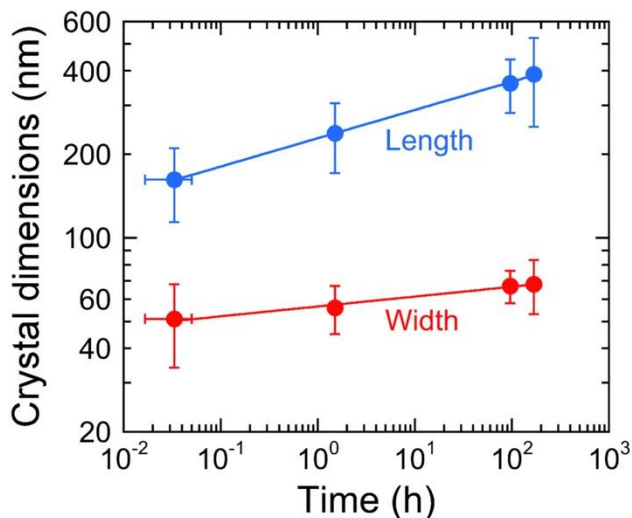


Figure 4. Crystal dimensions (labeled and color-coded) from TEM images (such as those displayed in **Figure 3**) of the ESEBE1 copolymer. The initial time is taken as 2 ± 1 min as the copolymer is quickly cooled from solution. The solid lines, obtained from power-law regressions of the data, serve as guides for the eye and suggest the existence of a scaling relationship with scaling exponents of 0.102 ± 0.002 (length) and 0.036 ± 0.003 (width).

the crystal dimensions measured directly from TEM images such as those presented in **Figure 3** are displayed as a function of isothermal solution-crystallization time in **Figure 4** and suggest that crystal growth exhibits a kinetic scaling relationship. Some of the crystals in **Figure 3c** continue to form a cusp, whereas most (but not all) of the crystals in **Figure 3d** are oriented parallel to the specimen surface. In specimen regions devoid of crystals in **Figures 3b-d**, background mottling is attributed to either self-assembly of the copolymer blocks and/or the formation of embryonic crystals.

The morphologies of the ESEBE1 and ESEBE2 copolymers subject to solution crystallization at different solution concentrations after being aged for 7 d at 25 °C have likewise been investigated by SAXS in **Figures 5a-b** and by WAXS in **Figures 5c-d**. According to **Figure 5a**, an unambiguous correlation peak at 0.84 nm^{-1} (which corresponds to $\approx 75 \text{ nm}$ according to Bragg's

law) develops when the solution concentration is at or exceeds 1 wt%. Despite the differences in molecular weight and composition between the two copolymers, a nearly identical structure factor peak is evident at all solution concentrations in **Figure 5b**. This observation is consistent with the expectation that the ESEBE2 copolymer is more readily able of crystallizing because of its lower molecular weight. Interestingly, the position of the peak is independent of solution concentration and compares surprisingly well with the width of the E crystals in the ESEBE1 copolymer after being aged for at least 4 days, as measured by TEM in **Figure 3**. At 5 and 10 wt% copolymer, a broad shoulder forms for both copolymers beyond the principal correlation peak in **Figures 5a-b**, indicating either a modest increase in long-range order or the presence of a second characteristic length scale attributed to the form factor. Similarly, the WAXS profiles in **Figures 5c-d** evince that crystallinity is detectable by the appearance of at least one reflection when the solution concentration is at least 5 wt% copolymer. As a benchmark, WAXS profiles acquired from bulk solution-cast copolymer films are included in **Figures 5c-d** and reveal the existence of scattering peaks representative of the (110) and (200) lattice projections of orthorhombic E at 15.0 and 16.6 nm⁻¹, respectively.⁴⁴ At 5 wt% ESEBE1 and higher, only the (110) reflection is observed, whereas both reflections are clearly discernible at 5 wt% ESEBE2 and higher. Since only the amorphous halo

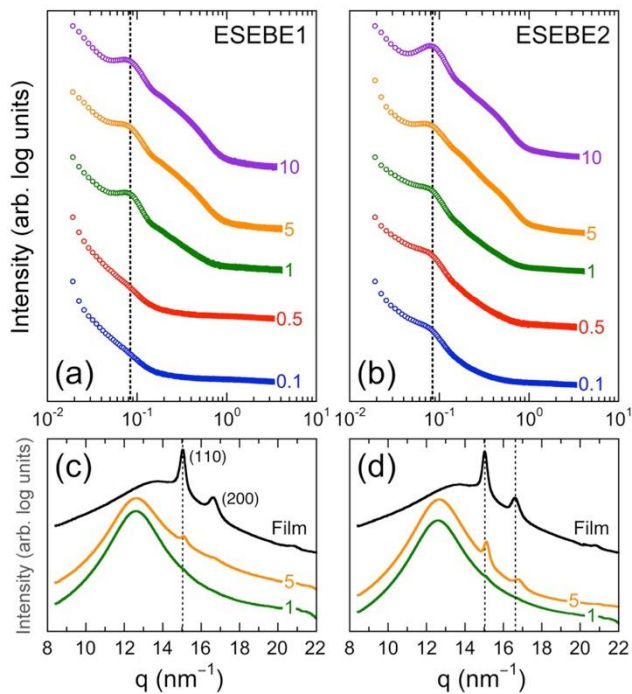


Figure 5. SAXS (a,b) and WAXS (c,d) profiles obtained from the ESEBE1 (a,c) and ESEBE2 (b,d) copolymers prepared at different solution concentrations (in wt%, labeled and color-coded) and aged for 7 d at 25 °C. The dotted line identifies the correlation peak. WAXS profiles measured from bulk films are included for reference and labeled in (c) and (d).

exists at lower copolymer concentrations, analysis of the WAXS profiles at 5 and 10 wt% copolymer indicates that X_c lies between 12 and 19% (slightly higher than values obtained from melt-processed films in **Table 1**), depending on copolymer grade and concentration.

The effect of solution temperature on morphological evolution is explored in **Figure 6**. Here, the initial solution is aged for 24 h at 98 °C. Upon cooling *in-situ* at 10 °C/min, no evidence of nanostructure development resulting in a correlation peak is apparent by SAXS at temperatures as low as 40 °C (cooling for 5.8 min). Shifted along the ordinate axis to facilitate discrimination in **Figure 6**,

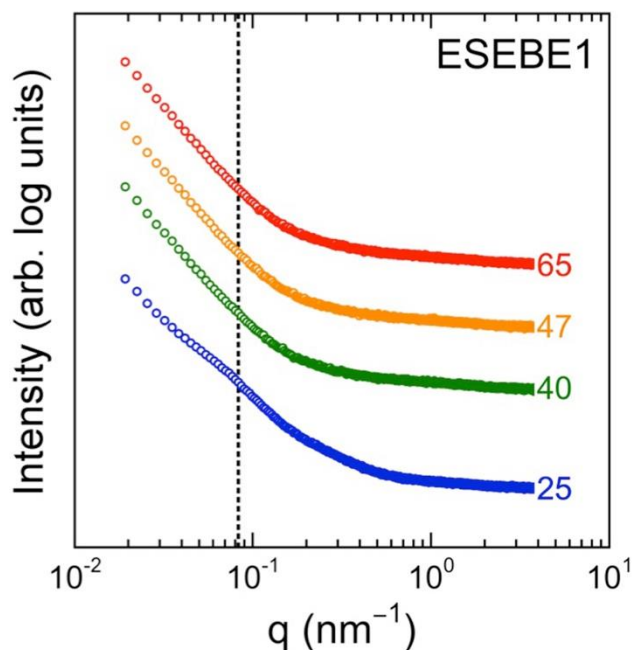


Figure 6. Temperature-dependent SAXS profiles collected from the ESEBE1 copolymer prepared at a solution concentration of 1 wt% and cooled from a homogeneous solution to 4 different temperatures (in °C, labeled and color-coded): 65, 47, 40, and 25. The dotted line identifies the position of the correlation peak in the aged solutions displayed in **Figure 5**.

three SAXS profiles acquired at temperatures above 25 °C are, in fact, all superposable, confirming that they represent homogeneous (unstructured) solutions. At 25 °C (cooling for 7.3 min), however, a broad scattering peak centered at the same q value as the structure factor peak evident in **Figure 5a** develops and presumably becomes increasingly refined upon aging. Our morphological results from microscopy and scattering consistently verify that the copolymers investigated here undergo concurrent self-assembly and endblock crystallization in solution over a wide range of copolymer concentrations, aging times and solution temperatures. Unlike crystallizable diblock copolymers that crystallize before (or concurrently with) self-assembly via CDSA,^{37,38} the current copolymers are triblock copolymers that, in the present solvent system,

appear to self-assemble first (due to solvent-incompatible midblocks) and subsequently crystallize, resulting in assembly-directed crystallization,²⁶ without the same midblock constraints encountered in conventional TPEs.¹³ The result is the formation of aggregates and films that display acicular crystals measuring up to *ca.* 400 nm long and 70 nm wide. Examination of the correlation peak in SAXS yields a characteristic dimension that is comparable to the width of the crystals.

When melt-processed, these TPEs are reported³⁹ to afford mechanical improvements over conventional styrenic TPEs. While our findings in this study establish that the early-stage morphologies of ESEBE copolymers depend on a balance between self-assembly and endblock crystallization during solution processing, a future comparison of crystallization mechanisms and outcomes from both solution- and melt-based processes can provide additional insight regarding this balance, as well as process-related differences related to molecular diffusion and segmental mobility. As a relatively new class of TPEs, these materials are resistant to oil and a wide range of organic solvents and are capable of compatibilizing polyolefins in blends and providing new routes to polyolefin recycling. Use of ESEBE copolymers for compatibilization of blends composed of a polyolefin and oil can yield elastic films for packaging, automotive skins and fabric/nonwoven coatings. An understanding of the competition between crystallization and self-assembly in this class of copolymers is clearly warranted in light of this application versatility.

Experimental Section

Two ESEBE triblock copolymers, synthesized by living anionic polymerization followed by hydrogenation, were provided by Kraton Corporation (Houston, TX). Reagent-grade cyclohexane was obtained from Fisher Scientific (Pittsburgh, PA), and ruthenium tetroxide (RuO₄, 0.5 wt% aqueous solution) was purchased from Electron Microscopy Sciences (Hatfield, PA). The molec-

ular weight characteristics of the copolymers were measured by high-temperature GPC, and copolymer compositions were determined from ^1H NMR spectroscopy performed on samples dissolved in *o*-dichlorobenzene at 100 °C with a Bruker Advance 400 spectrometer. Results from these measurements are listed in **Table 1**. Approximately 5-10 mL of each copolymer was dissolved in cyclohexane at different logarithmic concentrations in a 20 mL vial for 24 h at 98 °C, followed by two different cooling procedures: (i) slow-cooling to ambient temperature, and (ii) quenching to ambient temperature by submersion in a large water bath. For TEM, 10 μL of each polymer solution aged according to predetermined times and temperatures was drop-cast onto a carbon-supported 400-mesh copper grid (excess liquid was blotted). To enhance contrast between the microdomains and outline crystalline features, the specimens were subsequently exposed to the vapor of 0.5 wt% $\text{RuO}_4(\text{aq})$ solution for 7 min at ambient temperature in an isolated glass container to ensure staining of the aromatic rings. Images were acquired on a field-emission FEI Talos F200X microscope operated at an accelerating voltage of 80 kV. For SAXS, the polymer solutions were analyzed in thin-wall quartz capillary tubes, and the measurements were conducted on beamline 12-ID-B of the Advanced Photon Source at Argonne National Laboratory. Solutions were exposed to a 13.3 keV beam with a wavelength (λ) of 0.087 nm at a flux of $\sim 10^{12}$ photons/s for 1 s. Resultant 2D scattering patterns were azimuthally integrated to yield intensity profiles as a function of the scattering vector (q), where $q = (4\pi/\lambda)\sin\theta$ and θ denotes the scattering half-angle. For variable-temperature tests, the solutions were cooled at a rate of 10 °C/min.

Acknowledgments

This work was funded by the NC State Nonwovens Institute and used instrumentation maintained in the NC State Analytical Instrumentation Facility (AIF) with support from the National

Science Foundation (ECCS-1542015). The AIF is a member of the North Carolina Research Triangle Nanotechnology Network (RTNN), a site in the National Nanotechnology Coordinated Infrastructure (NNCI). This research used resources of the Advanced Photon Source, a U.S. Department of Energy (DOE) Office of Science User Facility operated for the DOE Office of Science by Argonne National Laboratory under Contract No. DE-AC02-06CH11357. The authors are grateful to Dr. J. E. Flood at Kraton Corporation for providing the copolymers.

References

1. Rogers, J. A.; Someya, T.; Huang, Y. Materials and Mechanics for Stretchable Electronics. *Science* **2010**, *327*, 1603–1607.
2. Dickey, M. D. Stretchable and Soft Electronics Using Liquid Metals. *Adv. Mater.* **2017**, *29*, 1606425.
3. Windmiller, J. R.; Wang, J. Wearable Electrochemical Sensors and Biosensors: A Review. *Electroanal.* **2013**, *25*, 29–46.
4. Kim, C.-C.; Lee, H.-H.; Oh, K. H.; Sun, J.-Y. Highly Stretchable, Transparent Ionic Touch Panel. *Science* **2016**, *353*, 682–687.
5. Wolf, M. P.; Salieb-Beugelaar, G. B.; Hunziker, P. PDMS with Designer Functionalities—Properties, Modifications Strategies, and Applications. *Prog. Polym. Sci.* **2018**, *83*, 97–134.
6. Shi, K.; Zou, H.; Sun, B.; Jiang, P.; He, J.; Huang, X. Dielectric Modulated Cellulose Paper/PDMS-Based Triboelectric Nanogenerators for Wireless Transmission and Electropolymerization Applications. *Adv. Funct. Mater.* **2020**, *30*, 1904536.
7. Zhong, M.; Wang, R.; Kawamoto, K.; Olsen, B. D.; Johnson, J. A. Quantifying the Impact of Molecular Defects on Polymer Network Elasticity. *Science* **2016**, *353*, 1264–1268.
8. Daniel, W. F. M.; Burdynska, J.; Vatankhah-Varnoosfaderani, M.; Matyjaszewski, K.; Paturej, J.; Rubinstein, M.; Dobrynin, A. V.; Sheiko, S. S. Solvent-Free, Supersoft and Superelastic Bottlebrush Melts and Networks. *Nat. Mater.* **2016**, *2*, 183–189.
9. Sheiko, S. S.; Dobrynin, A. V. Architectural Code for Rubber Elasticity: From Supersoft to Superfirm Materials. *Macromolecules* **2019**, *52*, 7531–7546.
10. Kubo, M.; Li, X. F.; Kim, C.; Hashimoto, M.; Wiley, B. J.; Ham, D.; Whitesides, G. M. Stretchable Microfluidic Radiofrequency Antennas. *Adv. Mater.* **2010**, *22*, 2749–2752.
11. Vatankhah-Varnoosfaderani, M.; Daniel, W. F. M.; Zhushma, A. P.; Li, Q.; Morgan, B. J.; Matyjaszewski, K.; Armstrong, D. P.; Spontak, R. J.; Dobrynin, A. V.; Sheiko, S. S. Bottlebrush Elastomers: A New Platform for Freestanding Electroactuation. *Adv. Mater.* **2017**, *29*, 1604209.

12. Holden, G.; Kricheldorf, H. R.; Quirk, R. P. *Thermoplastic Elastomers*, 3rd ed.; Hanser: Munich, 2004.
13. Tallury, S. S.; Spontak, R. J.; Pasquinelli, M. A. Dissipative Particle Dynamics of Triblock Copolymer Melts: A Midblock Conformational Study at Moderate Segregation. *J. Chem. Phys.* **2014**, *141*, 244911.
14. Yan, J.; Spontak, R. J. Advances in Stimuli-Responsive and Functional Thermoplastic Elastomers. In *Elastomer Blends and Composites: Principles, Characterizations, Advances and Applications* (M. R. Sanjay, J. Parameswaranpillai, S. Siengchin, and T. Ozbakkaloglu, eds.), Elsevier: Amsterdam; 2021, in press.
15. Wang, W.; Lu, W.; Goodwin, A.; Wang, H.; Yin, P.; Kang, N.-G.; Hong, K.; Mays, J. W. Recent Advances in Thermoplastic Elastomers from Living Polymerizations: Macromolecular Architectures and Supramolecular Chemistry. *Prog. Polym. Sci.* **2019**, *95*, 1–31.
16. TPE Market Approaches Maturity. *Plastics and Rubber Weekly*; October 18, 2016.
17. Hamersky, M. W.; Smith, S. D.; Gozen, A. O.; Spontak, R. J. Phase Behavior of Triblock Copolymers Varying in Molecular Asymmetry. *Phys. Rev. Lett.* **2005**, *95*, 168306.
18. Tallury, S. S.; Mineart, K. P.; Woloszczuk, S.; Williams, D. N.; Thompson, R. B.; Pasquinelli, M. A.; Banaszak, M.; Spontak, R. J. Molecular-Level Insights into Asymmetric Triblock Copolymers: Network and Phase Development. *J. Chem. Phys.* **2014**, *141*, 121103.
19. Petzetakis, N.; Stone, G. M.; Balsara, N. P. Synthesis of Well-Defined Polyethylene-Polydimethylsiloxane-Polyethylene Triblock Copolymers by Diimide-Based Hydrogenation of Polybutadiene Blocks. *Macromolecules* **2014**, *47*, 4151–4159.
20. Ashraf, A.; Ryan, J. J.; Satkowski, M. M.; Smith, S. D.; Spontak, R. J. Effect of Systematic Hydrogenation on the Phase Behavior and Nanostructural Dimensions of Block Copolymers. *ACS Appl. Mater. Interfaces* **2018**, *10*, 3186–3190.
21. Synatschke, C. V.; Nomoto, T.; Cabral, H.; Förtsch, M.; Toh, K.; Matsumoto, Y.; Miyazaki, K.; Hanisch, A.; Schacher, F. H.; Kishimura, A.; Nishiyama, N.; Müller, A. H. E.; Kataoka, K. Multicompartment Micelles with Adjustable Poly(ethylene glycol) Shell for Efficient In Vivo Photodynamic Therapy. *ACS Nano* **2014**, *8*, 1161–1172.
22. Schöbel, J.; Burgard, M.; Hils, C.; Dersch, R.; Dulle, M.; Volk, K.; Karg, M.; Greiner, A.; Schmalz, H. Bottom-Up Meets Top-Down: Patchy Hybrid Nonwovens as an Efficient Catalysis Platform. *Angew. Chem. Int. Ed.* **2017**, *56*, 405–408.
23. Lee, W.; Kim, G.-H.; Ko, S.-J.; Yum, S.; Hwang, S.; Cho, S.; Shin, Y.-H.; Kim, J. Y.; Woo, H. Y. Semicrystalline D–A Copolymers with Different Chain Curvature for Applications in Polymer Optoelectronic Devices. *Macromolecules* **2014**, *47*, 1604–1612.
24. Armstrong, D. P.; Spontak, R. J. Crystallization-Directed Anisotropic Electroactuation in Selectively-Solvated Olefinic Thermoplastic Elastomers: A Thermal and (Electro)Mechanical Property Study. *Adv. Funct. Mater.* **2018**, *28*, 1803467.
25. Gegenhuber, T.; Krekhova, M.; Schöbel, J.; Gröschel, A. H.; Schmalz, H. "Patchy" Carbon Nanotubes as Efficient Compatibilizers for Polymer Blends. *ACS Macro Lett.* **2016**, *5*, 306–310.

26. Loo, Y.-L.; Register, R. A.; Adamson, D. H. Polyethylene Crystal Orientation Induced by Block Copolymer Cylinders. *Macromolecules* **2000**, *33*, 8361–8366.
27. Loo, Y.-L.; Register, R. A.; Ryan, A. J. Modes of Crystallization in Block Copolymer Microdomains: Breakout, Templated, and Confined. *Macromolecules* **2002**, *35*, 2365–2374.
28. Arriola, D. J.; Carnahan, E. M.; Hustad, P. D.; Kuhlman, R. L.; Wenzel, T. T. Catalytic Production of Olefin Block Copolymers via Chain Shuttling Polymerization. *Science* **2006**, *312*, 714–719.
29. Li, S.; Register, R. A.; Weinhold, D.; Landes, B. G. Melt and Solid-State Structures of Polydisperse Polyolefin Multiblock Copolymers. *Macromolecules* **2012**, *45*, 5773–5781.
30. Myers, S. B.; Register, R. A. Extensibility and Recovery in a Crystalline–Rubbery–Crystalline Triblock Copolymer. *Macromolecules* **2009**, *42*, 6665–6670.
31. Schmalz, H.; Böker, A.; Lange, R.; Krausch, G.; Abetz, V. Synthesis and Properties of ABA and ABC Triblock Copolymers with Glassy (A), Elastomeric (B), and Crystalline (C) Blocks. *Macromolecules* **2001**, *34*, 8720–8729.
32. Zuo, F.; Alfonzo, C. G.; Bates, F. S. Structure and Mechanical Behavior of Elastomeric Multiblock Terpolymers Containing Glassy, Rubbery, and Semicrystalline Blocks. *Macromolecules* **2011**, *44*, 8143–8153.
33. Burns, A. B.; Register, R. A. Thermoplastic Elastomers via Combined Crystallization and Vitrification from Homogeneous Melts. *Macromolecules* **2016**, *49*, 269–279.
34. Beckingham, B. S.; Register, R. A. Synthesis and Phase Behavior of Block-Random Copolymers of Styrene and Hydrogenated Isoprene. *Macromolecules* **2011**, *44*, 4313–4319.
35. Ashraf, A. R.; Ryan, J. J.; Satkowski, M. M.; Lee, B.; Smith, S. D.; Spontak, R. J. Bicomponent Block Copolymers Derived from One or More Random Copolymers as an Alternative Route to Controllable Phase Behavior. *Macromol. Rapid Commun.* **2017**, *38*, 1700207.
36. Wang, X.; Guerin, G.; Wang, H.; Wang, Y.; Manners, I.; Winnik, M. A. Cylindrical Block Copolymer Micelles and Co-Micelles of Controlled Length and Architecture. *Science* **2007**, *317*, 644–647.
37. Gädt, T.; Jeong, N. S.; Cambridge, G.; Winnik, M. A.; Manners, I. Complex and Hierarchical Micelle Architectures from Diblock Copolymers Using Living, Crystallization-Driven Polymerizations. *Nat. Mater.* **2009**, *8*, 144–150.
38. Lunn, D. J.; Gould, O. E. C.; Whittell, G. R.; Armstrong, D. P.; Mineart, K. P.; Winnik, M. A.; Spontak, R. J.; Pringle, P. G.; Manners, I. Microfibers and Macroscopic Films from the Coordination-Driven Hierarchical Self-Assembly of Cylindrical Micelles. *Nat. Commun.* **2016**, *7*, 12371.
39. Flood, J. E.; Tan, K.; Muyltermans, X.; McGilbert, S. K.; Culbert, L. A New Semi-Crystalline Styrenic Block Copolymer for Elastic Films, Fibers and Compounds. Presented at the 2017 SPE International Polyolefins Conference, Houston, TX, 2017.
40. Fetters, L. J.; Lohse, D. J.; Richter, D.; Witten, T. A.; Zirkel, A. Connection between Polymer Molecular-Weight, Density, Chain Dimensions, and Melt Viscoelastic Properties. *Macromolecules* **1994**, *27*, 4639–4647.

41. Young, R. J.; Lovell, P. A. *Introduction to Polymers, 3rd Ed.*; CRC Press: Boca Raton, FL; 2011, p. 252.
42. Oliver, A. M.; Spontak, R. J.; Manners, I. Solution Self-Assembly of ABC Triblock Terpolymers with a Central Crystallizable Poly(ferrocenyldimethylsilane) Core-Forming Segment. *Polym. Chem.* **2019**, *10*, 2559–2569.
43. Cheng, S.; Hu, Y.; Wu, X.; Li, W.; Mu, J. Hierarchical Self-Assembly of Polyethylene Mid-block Copolymers in Hot Steam: Key Role of Crystalline and Topological Structure. *Macromol. Chem. Phys.* **2021**, 2000419.
44. Romo-Uribe, A.; Manzur, A.; Olayo, R. Synchrotron Small-Angle x-Ray Scattering Study of Linear Low-Density Polyethylene under Uniaxial Deformation. *J. Mater. Res.* **2012**, *27*, 1351–1359.